ARTICLE

Behavioral, circuitry, and molecular aberrations by region-specific deficiency of the high-risk autism gene *Cul3*

Maximiliano Rapanelli[1] · Tao Tan[1] · Wei Wang[1] · Xue Wang[2] · Zi-Jun Wang[1] · Ping Zhong[1] · Luciana Frick[3] · Luye Qin[1] · Kaijie Ma[1] · Jun Qu[2] · Zhen Yan [1]

Abstract

Cullin 3 (Cul3) gene, which encodes a core component of the E3 ubiquitin ligase complex that mediates proteasomal degradation, has been identified as a true high-risk factor for autism. Here, by combining behavioral, electrophysiological, and proteomic approaches, we have examined how Cul3 deficiency contributes to the etiology of different aspects of autism. Heterozygous mice with forebrain Cul3 deletion displayed autism-like social interaction impairment and sensory-gating deficiency. Region-specific deletion of Cul3 leads to distinct phenotypes, with social deficits linked to the loss of Cul3 in prefrontal cortex (PFC), and stereotypic behaviors linked to the loss of Cul3 in striatum. Correlated with these behavioral alterations, Cul3 deficiency in forebrain or PFC induces NMDA receptor hypofunction, while Cul3 loss in striatum causes a cell type-specific alteration of neuronal excitability in striatal circuits. Large-scale profiling has identified sets of misregulated proteins resulting from Cul3 deficiency in different regions, including Smyd3, a histone methyltransferase involved in gene transcription. Inhibition or knockdown of Smyd3 in forebrain *Cul3*-deficient mice ameliorates social deficits and restores NMDAR function in PFC. These results have revealed for the first time a potential molecular mechanism underlying the manifestation of different autism-like behavioral deficits by Cul3 deletion in cortico-striatal circuits.

Introduction

Autism is a neurodevelopmental disorder diagnosed on the basis of core behavioral abnormalities like social deficits and stereotypic behaviors. A complex genetic framework of mutations and/or chromosomal deletions/duplications have been linked to autism spectrum disorder (ASD) [1, 2].

✉ Zhen Yan
zhenyan@buffalo.edu

1 Department of Physiology and Biophysics, Jacobs School of Medicine and Biomedical Sciences, State University of New York at Buffalo, Buffalo, NY, USA

2 New York State Center of Excellence in Bioinformatics and Life Sciences, Buffalo, NY, USA

3 Hunter James Kelly Research Institute, Department of Neurology, State University of New York at Buffalo, Buffalo, NY, USA

Recurrent de novo loss-of-function mutations on the *Cullin 3* (*Cul3*) gene were found in different cohorts of autism patients by large-scale unbiased genetic screening [3, 4], making Cul3 one of the top-ranking high-risk autism factors [2, 5]. These individuals have one normal allele and one nonfunctional allele, resulting in the capacity to make less Cul3. *Cul3* encodes a core component of the E3 ubiquitin ligase complex, which is responsible for the recognition and recruitment of substrates that need to be ubiquitinylated and degraded [6, 7]. By working with many BTB domain-containing substrate adapters, Cul3 is involved in a plethora of processes, including cytoskeleton organization, cell differentiation, arterial pressure control, and cellular stress responses [6, 8, 9]. One of the Cul3 adapters, *Kctd13* [7], is located at the 16p11.2 gene locus, and either 16p11.2 deletions or duplications have been linked to autism [10, 11] and schizophrenia [12].

Despite the discovery of *Cul3* as a strong autism candidate gene [2, 4], there is little information about how *Cul3* haploinsufficiency contributes to the pathophysiology of ASD. Whole-body deletion of *Cul3* leads to lethality in mice [13], which has hampered the discovery of in vivo functions of Cul3 in neurons. In this study, we examined

behavioral, synaptic, and molecular alterations resulting from *Cul3* deficiency in the forebrain, since forebrain dysfunction has been found in patients with autism [14–16]. A growing body of evidence points to cortico-striatal alterations as being responsible for ASD symptoms [17, 18]. Thus, we also knocked out *Cul3* in prefrontal cortex (PFC) or striatum, and examined the multilevel impact.

Materials and methods

Animals, stereotaxic surgery, and viral injection

All animal studies were performed with the approval of the Institutional Animal Care and Use Committee (IACUC) of the State University of New York at Buffalo. Cul3$^{flox/fox}$ mice from Jackson Laboratory (stock #: 028349) were bred with Emx1-IRES-Cre mice (stock #: 005628) to generate forebrain-specific Cul3 knockout mice (Cul3$^{f/-}$). Both male and female Cul3$^{f/-}$ and Cul3$^{f/f}$ mice were used in this study. Animals were group housed with food and water ad libitum under a 12/12-h light/dark cycle. Animals were randomly assigned to experimental groups after genotyping. Investigators were blinded to the group allocation (with no prior knowledge about the genotypes and treatments) during experiments. Mice were 4 weeks old at the time of surgery. All behavioral testing, electrophysiological recording, or tissue harvesting procedures were performed at the age of 6 weeks old.

Cul3$^{flox/fox}$ mice were deeply anesthetized with ketamine/xylazine (100 mg/kg; 10 mg/kg) and placed in a mouse stereotaxic frame (Stoelting, USA). Under standard and sterile surgical conditions, a 10 μl syringe (7000 series, Hamilton, USA) attached to a micropump was lowered through to skull burr hole into the PFC (AP + 1.8 mm, L ± 0.3 mm, DV − 2.7 mm) or the striatum (AP + 1 mm, L ± 1.5 mm, DV − 2.7 mm). Mice were injected with either AAV8-CaMKIIα-GFP-Cre or AAV8-CaMKIIα-GFP (1×10^{13}, UNC Viral Core, USA) in the PFC (0.3 μl per hemisphere) or striatum (0.5 μl per hemisphere) at a flow rate of 50 nl/min.

Behavioral procedures

Details for behavioral studies, including social preference and social engagement tests, locomotion, open-field, rotarod test, stereotypic self-grooming test, startle response, and pre-pulse inhibition (PPI) test, are included in Supplementary Methods.

Electrophysiological recordings

Details for whole-cell patch-clamp recordings in brain slices are included in Supplementary Methods.

Immunofluorescence and confocal imaging

See Supplementary Methods for details.

Western blotting of total, synaptic, and nuclear proteins

See Supplementary Methods for details.

Golgi staining, sholl analysis, and spine counting

See Supplementary Methods for details.

Proteomic analysis and bioinformatics

See Supplementary Methods for details.

Drug administration and knockdown

Details for the administration of Smyd3 inhibitor and Smyd3 shRNA lentivirus are included in Supplementary Methods.

Statistics

Statistical analyses were performed with GraphPad Prism 6 (GraphPad Software, Inc., La Jolla, CA). All data were expressed as the mean ± SEM. No sample was excluded from the analysis. The sample size was based on power analyses and was similar to those reported in previous works. The variance between groups being statistically compared was similar. Each set of the experiments was replicated at least three times. Experiments with two groups were analyzed statistically using Student's *t* tests. Experiments with more than two groups were subjected to one-way ANOVA, two-way ANOVA, or two-way repeated measure ANOVA (rmANOVA), followed by post hoc Bonferroni tests. For data with non-normal distribution, nonparametric statistical analysis were performed with Kruskal–Wallis (K–W) tests to compare more than two groups and Mann–Whitney tests to compare two groups.

Results

Brain region-specific Cul3 deficiency induces distinct behavioral phenotypes associated with autism

Children with autism exhibit neocortical disorganization with the clearest abnormality in the markers of deep layer glutamatergic pyramidal neurons [16], so we generated forebrain-specific Cul3 knockout mice by crossing Cul3$^{flx/flx}$ (*loxP*::*frt*-neo-*frt*::exons4–7::*loxP*) mice, in which a Cul3
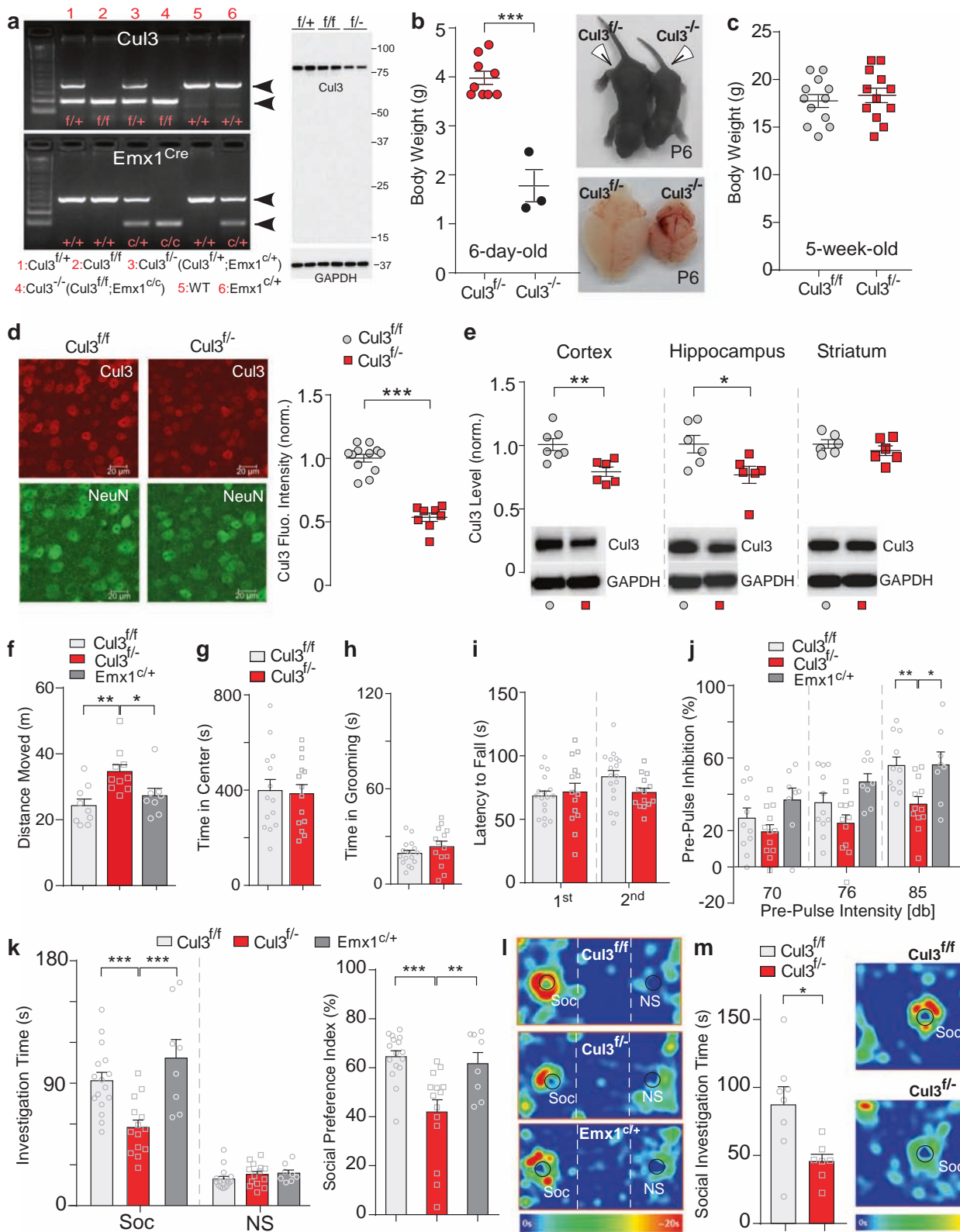
hypomorphic allele is converted to a null allele after Cre recombinase exposure [19], with Emx1-IRES-Cre knockin mice, which have endogenous *Emx1* locus directing expression of Cre recombinase to cortical excitatory glutamatergic neurons, but not inhibitory GABAergic interneurons, and other forebrain structures, including the

Fig. 1 Forebrain Cul3 deficiency produces autism-associated behavioral phenotypes. **a** PCR images showing the genotyping of forebrain Cul3 knockout mice and controls. Inset: A full immunoblot showing Cul3 protein expression in frontal cortex of Cul3 floxed mice, Cul3$^{f/+}$ and Cul3$^{f/f}$, as well as heterozygous forebrain Cul3 KO mice Cul3$^{f/-}$ (Emx1$^{Cre/+}$; Cul3$^{f/+}$). **b, c** Plots and images showing the body weight and brain size of Cul3$^{f/-}$ (heterozygous forebrain Cul3 KO), Cul3$^{-/-}$ (homozygous forebrain Cul3 KO), and Cul3$^{f/f}$ (control) mice. **b** $t(10) = 10.6$, $p < 0.001$, t test. **d** Representative confocal images of Cul3 (red) and NeuN (green) staining and quantification of Cul3 expression levels in the frontal cortex of Cul3$^{f/f}$ ($n = 12$ slices/6 mice) and Cul3$^{f/-}$ ($n = 8$ slices/4 mice). $t(18) = 10.0$, $p < 0.001$, t test. **e** Western blot assay of the Cul3 level in cortex, hippocampus and striatum from Cul3$^{f/f}$ ($n = 6$–7) and Cul3$^{f/-}$ ($n = 6$) mice. Cortex: $t(11) = 3.5$, $p = 0.005$, t test; Hippocampus: $t(10) = 2.5$, $p = 0.03$, t test. **f** Plot of total distance moved in the locomotion test of Cul3$^{f/f}$ ($n = 14$), Cul3$^{f/-}$ ($n = 14$), and Emx1-Cre (Emx1$^{c/+}$, $n = 8$) mice. $F_{(2,24)} = 6.7$, $p = 0.005$, one-way ANOVA. **g** Plot of time in center in open-field tests of Cul3$^{f/f}$ ($n = 14$) and Cul3$^{f/-}$ ($n = 14$) mice. **h** Plot of time spent on repetitive grooming in Cul3$^{f/f}$ ($n = 16$) and Cul3$^{f/-}$ ($n = 14$) mice. **i** Plot of the latency to fall in rotarod tests of Cul3$^{f/f}$ ($n = 17$) and Cul3$^{f/-}$ ($n = 14$) mice. **j** Plot of pre-pulse inhibition of startle responses measured at three different intensities in Cul3$^{f/f}$ ($n = 11$), Cul3$^{f/-}$ ($n = 12$), and Emx1$^{c/+}$ ($n = 8$) mice. $F_{(2,28)genotype} = 4.9$, $p = 0.015$; $F_{(2,56)prepulse} = 63.4$, $p < 0.001$; $F_{(4,56)interaction} = 3.2$, $p = 0.02$; two-way rmANOVA. **k** Plot of the time investigating social (Soc) vs. nonsocial (NS) stimuli and social preference index in three-chamber sociability tests of Cul3$^{f/f}$ ($n = 13$), Cul3$^{f/-}$ ($n = 14$), and Emx1$^{c/+}$ ($n = 8$) mice. Investigation time: $F_{(2,70)genotype} = 9.8$, $p = 0.002$; $F_{(1,70)stimulus} = 185.6$, $p < 0.001$; $F_{(2,70)interaction} = 10.6$, $p < 0.001$, two-way ANOVA; Social preference index: $F_{(2,35)} = 10.3$, $p < 0.001$, one-way ANOVA. **l** Representative heat maps of Cul3$^{f/f}$, Cul3$^{f/-}$, and Emx1$^{c/+}$ mice illustrating the time spent in different locations of the three chambers from social preference tests. Locations of Soc and NS stimuli are labeled with the circles. **m** Plot of the time investigating Soc stimulus in social engagement tests of Cul3$^{f/f}$ ($n = 8$) and Cul3$^{f/-}$ ($n = 7$) mice. $t(13) = 2.7$, $p = 0.02$, t test. Inset: Representative heat maps

hippocampus and amygdala [20, 21]. Representative genotyping is shown in Fig. 1a. Cul3 floxed mice, Cul3$^{f/f}$ and Cul3$^{f/+}$, had a similar level of Cul3 in frontal cortex (Fig. 1a), so Cul3$^{f/f}$ mice were used as the control. Heterozygous forebrain Cul3 KO mice (Emx1$^{Cre/+}$; Cul3$^{f/+}$, referred as Cul3$^{f/-}$) had normal growth, while homozygous forebrain Cul3 KO mice (Emx1$^{Cre/Cre}$; Cul3$^{f/f}$, referred as Cul3$^{-/-}$) had smaller body weight and brain size and died within one week after birth (Fig. 1b, c). Thus, Cul3$^{f/-}$ mice (6–7 weeks old) were used in this study.

To confirm Cul3 deficiency in Cul3$^{f/-}$ mice, we first performed quantitative immunostaining to examine the expression level of Cul3 in the forebrain. As shown in Fig. 1d, the Cul3 level was significantly decreased in frontal cortical neurons from Cul3$^{f/-}$ mice, compared to those from Cul3$^{f/f}$ control mice. Quantitative Western blotting also showed the diminished level of Cul3 in cortical and hippocampal lysates from Cul3$^{f/-}$ mice (Fig. 1e).

Behavioral assays found that Cul3$^{f/-}$ mice (6 week old) displayed increased locomotion, compared to Cul3$^{f/f}$ control mice or Emx1-Cre mice (Fig. 1f). They had no anxiety-like behaviors in the open-field test (Fig. 1g). Repetitive grooming, a stereotypic behavior associated with ASD, was not observed in Cul3$^{f/-}$ mice (Fig. 1h). Motor coordination, as measured by rotarod test, was normal in Cul3$^{f/-}$ mice (Fig. 1i).

Sensorimotor gating deficits, which are present in adults with autism [22], were also tested by measuring PPI of the acoustic startle, in which a weaker acoustic pre-stimulus inhibits the reaction to a subsequent strong startling stimulus. While Cul3$^{f/-}$ mice exhibited normal startle responses, PPI was significantly reduced at the highest stimulus intensity in Cul3$^{f/-}$ mice (Fig. 1j), compared to Cul3$^{f/f}$ or Emx1-Cre mice, suggesting the impairment of sensorimotor gating by forebrain Cul3 deficiency.

In the three-chamber social preference test, Cul3$^{f/-}$ mice spent significantly less time interacting with the social stimulus and had a significantly lower social preference index (Fig. 1k, l), compared to their counterparts, Cul3$^{f/f}$ mice. Emx1-Cre mice had normal social preference (Fig. 1k, l). In the direct social engagement test, Cul3$^{f/-}$ mice also spent significantly less time approaching and interacting with the social stimulus than Cul3$^{f/f}$ control mice (Fig. 1m). These results indicate that forebrain deletion of Cul3 leads to the manifestation of social interaction impairment, one of the main behavioral characteristics of ASD.

To find out the key brain regions that may mediate the behavioral phenotypes of forebrain Cul3-deficient mice, we used viral transfer to achieve the specific knockout of Cul3 in the PFC, a central region contributing to autism-associated abnormalities [23–27]. To target PFC pyramidal neurons specifically, a CaMKIIα-driven Cre virus or a GFP control virus was stereotaxically injected bilaterally into the medial PFC of Cul3$^{f/f}$ mice. As shown in Fig. 2a, most of the Cre virus-infected PFC pyramidal neurons lost the expression of Cul3. Western blot analyses also indicated the significantly reduced level of Cul3 in the cell lysates from infected PFC regions (Fig. 2b).

Mice with PFC-specific deletion of Cul3, Cul3$^{f/f}$ + Cre (PFC), spent significantly less time interacting with the social stimulus and had a significantly lower social preference index in the three-chamber sociability test, compared to GFP-injected control mice, Cul3$^{f/f}$ + GFP(PFC) (Fig. 2c, d). No change in social behaviors was found in WT mice injected with the Cre virus (Fig. 2c), ruling out potential non-specific effects from surgical intervention. Cul3$^{f/f}$ + Cre(PFC) mice exhibited normal locomotor activity and normal motor coordination (Supplementary Fig. 1a and b). They had no anxiety-like behaviors or stereotypic repetitive grooming behavior (Supplementary Fig. 1c and d). Normal startle responses and PPI (Supplementary Fig. 1e and f) were also observed in these mice. Therefore, only the autism-like social deficits are commonly induced by forebrain Cul3 deficiency or PFC-specific knockout of Cul3.
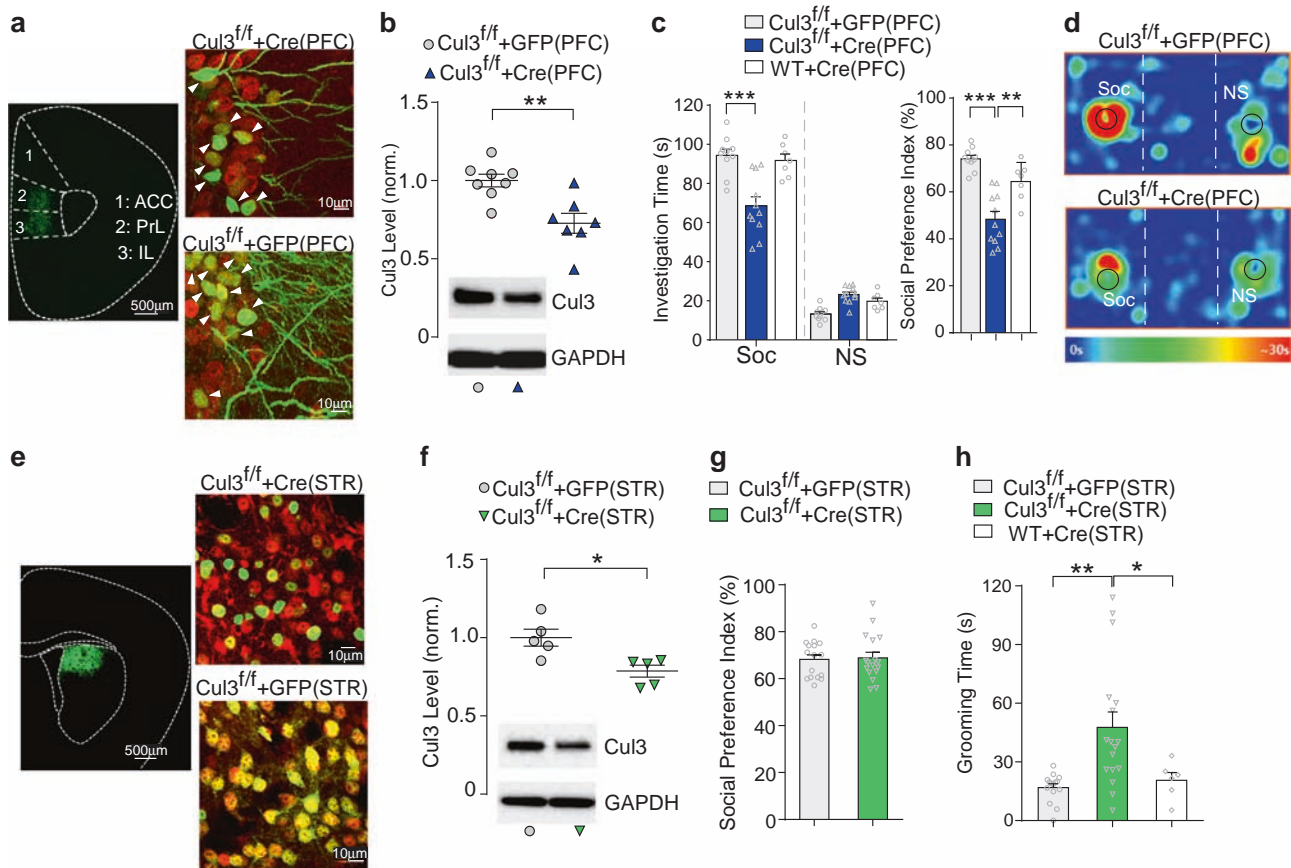
Fig. 2 Prefrontal cortex- or striatum-specific Cul3 deficiency leads to social deficits or repetitive behaviors, respectively. **a** Confocal images of Cul3 immunostaining (red) and GFP in PFC slices from Cul3$^{f/f}$ mice with the PFC injection of AAV8-CaMKIIα-GFP-Cre (Cul3$^{f/f}$ + Cre (PFC)) or AAV8-CaMKIIα-GFP (Cul3$^{f/f}$ + GFP(PFC)). Arrows point to GFP + neurons. A low-magnification image of PFC-containing slice illustrating the viral-infected area is also shown (PrL prelimbic, IL Infralimbic, ACC anterior cingulate cortex). **b** Western blot assay of Cul3 levels in PFC lysates from Cul3$^{f/f}$ + GFP(PFC) ($n = 8$) and Cul3$^{f/f}$ + Cre(PFC) mice ($n = 7$). $t(13) = 3.7$, $p = 0.003$, t test. **c** Plot of investigation time with Soc vs. NS stimuli and social preference index in three-chamber sociability tests of Cul3$^{f/f}$ + GFP(PFC) mice ($n = 10$), Cul3$^{f/f}$ + Cre(PFC) mice ($n = 11$), and WT mice with Cre virus injection to PFC (WT + Cre(PFC), $n = 7$). Investigation time: $F_{(2,50)\text{genotype}} = 6.5$, $p = 0.003$; $F_{(1,50)\text{stimulus}} = 728.9$, $p < 0.001$; $F_{(2,50)\text{interaction}} = 22.3$, $p < 0.001$, two-way ANOVA; social preference

index: $F_{(2,25)} = 24.3$, $p < 0.001$, one-way ANOVA. **d** Representative heat maps of Cul3$^{f/f}$ + GFP(PFC) and Cul3$^{f/f}$ + Cre(PFC) mice. **e** Confocal images of Cul3 immunostaining (red) and GFP in striatal slices from Cul3$^{f/f}$ mice with the striatal injection of AAV8-CaMKIIα-GFP-Cre (Cul3$^{f/f}$ + Cre(STR)) or AAV8-CaMKIIα-GFP (Cul3$^{f/f}$ + GFP(STR)). A low-magnification image of dorsal striatum-containing slice illustrating the viral-infected area is also shown. **f** Western blot assay of Cul3 levels in striatal lysates from Cul3$^{f/f}$ + GFP(STR) ($n = 5$) and Cul3$^{f/f}$ + Cre(STR) mice ($n = 5$). $t(8) = 3.2$, $p = 0.01$, t test. **g** Plot of social preference index in three-chamber sociability test of Cul3$^{f/f}$ + GFP(STR) ($n = 16$) and Cul3$^{f/f}$ + Cre(STR) mice ($n = 17$). **h** Plot of time spent on repetitive grooming in Cul3$^{f/f}$ + GFP(STR) mice ($n = 15$), Cul3$^{f/f}$ + Cre(STR) mice ($n = 17$), and WT mice with Cre virus injection to the striatum (WT + Cre(STR), $n = 6$). $F_{(2,35)} = 8.2$, $p = 0.0012$, one-way ANOVA. In all figures, *$p < 0.05$, **$p < 0.01$, ***$p < 0.001$

To further explore the behavioral consequences of region-specific Cul3 knockout, we injected the CaMKIIα-driven Cre virus or a GFP control virus bilaterally into dorsal striatum, an area linked to ASD-like stereotypic behaviors [28–30]. The expression of Cul3 was greatly diminished in Cre virus-infected striatal medium spiny neurons (Fig. 2e). Western blotting analyses of the infected striatal regions also found a significant reduction of the Cul3 level (Fig. 2f).

Mice with striatum-specific deletion of Cul3, Cul3$^{f/f}$ + Cre(STR), exhibited no difference in social preference index in the three-chamber sociability test, compared to GFP-injected control mice, Cul3$^{f/f}$ + GFP(STR) (Fig. 2g).

However, Cul3$^{f/f}$ + Cre(STR) mice exhibited significantly increased repetitive grooming (Fig. 2h), another core ASD-like behavior. No increased grooming was found in WT mice injected with the Cre virus (Fig. 2h). Cul3$^{f/f}$ + Cre (STR) mice had normal locomotor activity, normal motor coordination (Supplementary Fig. 2a and b), and no anxiety-like behaviors (Supplementary Fig. 2c). In addition, these mice had normal startle responses and no PPI deficits (Supplementary Fig. 2d and e). Cul3$^{f/f}$ + Cre(STR) mice showed normal social interaction time (Supplementary Fig. 2f and g). Thus, striatum-specific knockout of Cul3 only induces the autism-like stereotypic behavior.
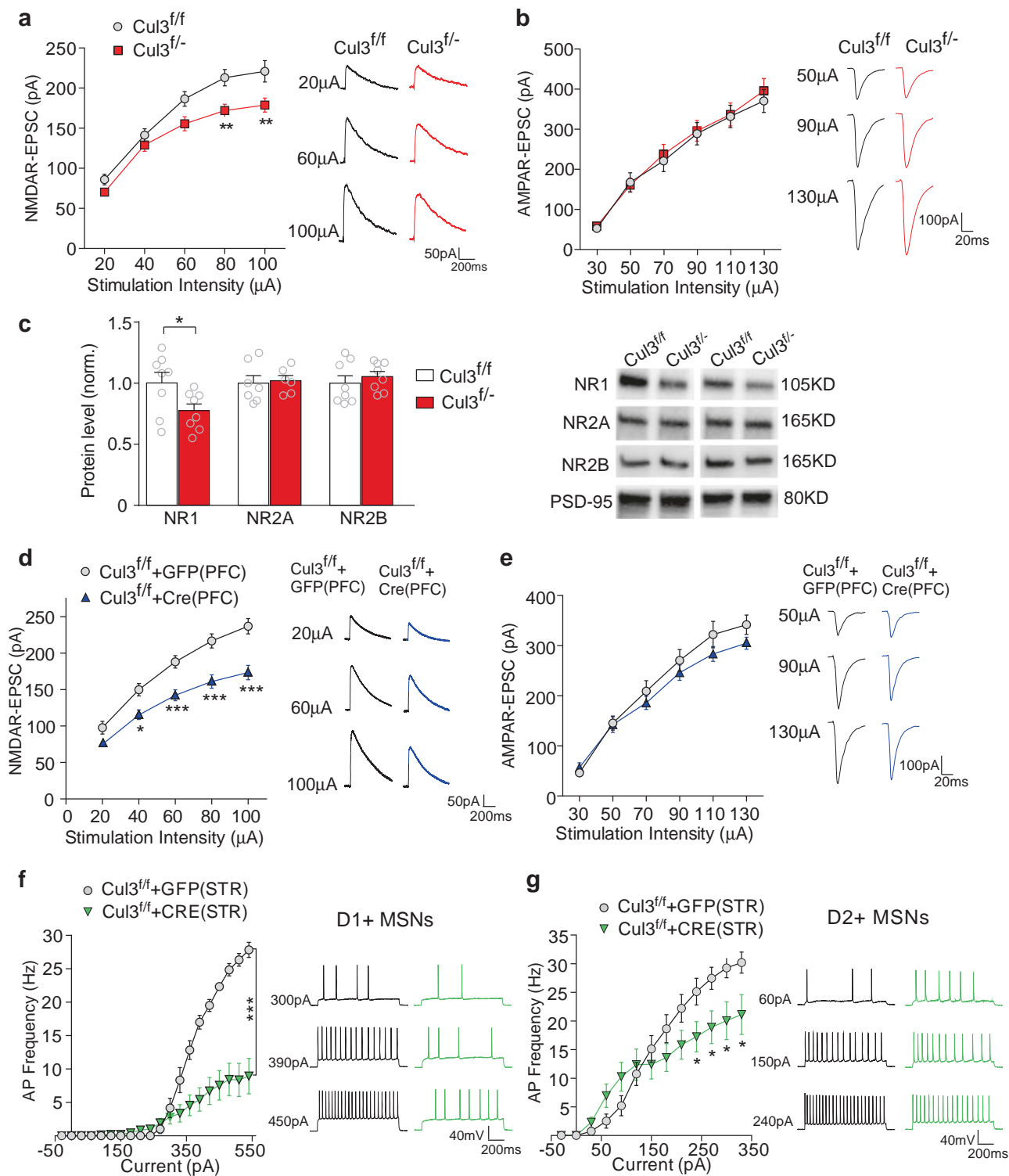
Brain region-specific Cul3 deficiency causes NMDA receptor hypofunction in PFC and neuronal excitability attenuation in striatum

To understand the physiologic basis of the behavioral phenotypes in mice with region-specific Cul3 deficiency,

we performed whole-cell patch–clamp recordings to measure synaptic currents and action potential (AP) firing. In mice with forebrain-specific Cul3 deletion (Cul3$^{f/-}$), the amplitudes of NMDAR-mediated excitatory postsynaptic currents (EPSC) evoked by a series of stimulus intensities in frontal cortical pyramidal neurons were significantly

Fig. 3 Cul3 deletion alters synaptic function and neuronal excitability in a cell type-specific manner. **a, b** Input/output curves of NMDAR-EPSC (**a**) and AMPAR-EPSC (**b**) in layer five frontal cortical pyramidal neurons from Cul3$^{f/f}$ and Cul3$^{f/-}$ mice. **a** $F_{(1,45)genotype} = 6.9$, $p = 0.01$; $F_{(4,180)stimulus} = 235.9$, $p < 0.001$; $F_{(4,180)interaction} = 4.6$, $p = 0.002$, two-way rmANOVA, $n = 23–24$ cells/6 pairs of mice; **b** $n = 12–16$ cells/4 pairs of mice. **c** Western blot assay of NMDAR subunits (NR1, NR2A, and NR2B) in the synaptic fraction of frontal cortical lysates from Cul3$^{f/f}$ ($n = 7–8$) and Cul3$^{f/-}$ ($n = 6–8$) mice. NR1: $t(14) = 2.2$, $p = 0.04$, t test. **d, e** Input/output curves of NMDAR-EPSC (**d**) and AMPAR-EPSC (**e**) in GFP-positive layer five PFC pyramidal neurons from Cul3$^{f/f}$ + GFP(PFC) and Cul3$^{f/f}$ + Cre (PFC) mice. **d** $F_{(1,54)genotype} = 16.4$, $p < 0.001$; $F_{(4,216)stimulus} = 260.3$, $p < 0.001$; $F_{(4,216)interaction} = 7.5$, $p < 0.001$, two-way rmANOVA, $n = 24-32$ cells/5–7 mice per group; **e** $n = 11–12$ cells/3–4 mice per group. **f, g** Plot of AP frequency in response to injected currents in putative D1-positive MSNs (**e**) and D2-positive MSNs (**f**) from Cul3$^{f/f}$ + GFP (STR) and Cul3$^{f/f}$ + Cre(STR) mice. **f** $F_{(1,18)genotype} = 15.0$, $p < 0.001$; $F_{(19,342)current} = 62.8$, $p < 0.001$; $F_{(19,342)interaction} = 17.4$, $p < 0.001$, two-way rmANOVA, $n = 6$ cells/3 mice, **g** $F_{(1,34)genotype} = 1.6$, $p = 0.2$; $F_{(12,408)current} = 56.9$, $p < 0.001$; $F_{(12,408)interaction} = 4.5$, $p < 0.001$, two-way rmANOVA, $n = 14$ cells/4 mice; representative traces are presented in (**a**, **b**, **d**, **e**, **f**, **g**) panels. In all figures, $*p < 0.05$, $**p < 0.01$, $***p < 0.001$

decreased, compared to Cul3$^{f/f}$ controls (Fig. 3a). The decay kinetics of NMDAR-EPSC, a parameter associated with the relative contribution of NR2A vs. NR2B subunits, was similar in Cul3$^{f/f}$ vs. Cul3$^{f/-}$ mice. The input–output (I/O) curves of AMPAR-EPSC were unchanged in Cul3$^{f/-}$ mice (Fig. 3b). The paired-pulse ratio (PPR) of NMDAR-EPSC or AMPAR-EPSC, a measure of pre-synaptic changes, was not altered by the forebrain loss of Cul3 (Supplementary Fig. 3a and b). The frequency of synaptic-driven, spontaneous AP (sAP) and the resting membrane potential (RMP) were also normal in Cul3$^{f/-}$ mice (Supplementary Fig. 3c).

To find out the molecular basis for NMDAR hypofunction in forebrain Cul3-deficient mice, we examined the expression level of synaptic NMDAR subunits. As shown in Fig. 3c, NR1 subunits in the synaptic fraction of frontal cortical tissues were significantly reduced in Cul3$^{f/-}$ mice, compared to Cul3$^{f/f}$ mice, while synaptosomal NR2A and NR2B subunits were largely unchanged. It suggests that the reduced amount of synaptic NMDARs may underlie the reduction of NMDAR-EPSC in forebrain Cul3-deficient mice.

In mice with PFC deletion of Cul3, Cul3$^{f/f}$ + Cre(PFC), a profound reduction of NMDAR-EPSC in PFC pyramidal neurons was detected, compared to GFP virus-injected controls, Cul3$^{f/f}$ + GFP(PFC) (Fig. 3d). Cul3$^{f/f}$ + Cre(PFC) mice exhibited no significant changes in the I/O of AMPAR-EPSC (Fig. 3e), PPR of NMDAR-EPSC, PPR of AMPAR-EPSC (Supplementary Fig. 3d and e), or the frequency of sAP and RMP (Supplementary Fig. 3f). Thus, only NMDAR hypofunction is induced by forebrain Cul3 deficiency or PFC-specific knockout of Cul3.

In mice with striatal deletion of Cul3, Cul3$^{f/f}$ + Cre (STR), we first examined the changes in neuronal excitability. AP evoked by the injection of a series of depolarizing currents in striatal medium spiny neurons (MSNs) from Cul3$^{f/f}$ + Cre(STR) mice were compared to those from GFP virus-injected controls, Cul3$^{f/f}$ + GFP(STR). We found two groups of MSNs with strikingly different AP thresholds and frequencies, consistent with the electrophysiological properties of striatonigral dopamine D1 receptor-expressing MSNs (D1+) vs. striatopallidal dopamine D2 receptor-expressing MSNs (D2+) [31, 32]. In putative D1 + MSNs, which required high depolarizing currents (>250pA) for firing AP, a huge reduction in the AP frequency was detected in Cul3$^{f/f}$ + Cre(STR) mice (Fig. 3f). In putative D2 + MSNs, which required low depolarizing currents (<50pA) for firing AP, only a small reduction in the AP frequency evoked by large depolarizing currents was detected in Cul3$^{f/f}$ + Cre(STR) mice (Fig. 3g). No significant alteration of membrane resistance in D1+ or D2 + MSNs of Cul3$^{f/f}$ + Cre(STR) mice was detected. These data suggest that the excitability of D1+ striatonigral MSNs is more prominently diminished by Cul3 deletion.

We next examined the impact of striatal deletion of Cul3 on synaptic currents in MSNs. The amplitudes of GABA$_A$R-mediated inhibitory postsynaptic currents (IPSC) evoked by a series of stimulus intensities in Cul3$^{f/f}$Cre(STR) mice were largely unchanged, compared to GFP virus-injected controls (Supplementary Fig. 4a). The PPR of IPSC was also not altered (Supplementary Fig. 4b). No significant differences were found in the frequency and amplitude of spontaneous IPSC in MSNs from Cul3$^{f/f}$ + Cre(STR) vs. Cul3$^{f/f}$ + GFP(STR) mice (Supplementary Fig. 4c). The amplitudes of AMPAR-EPSC and NMDAR-EPSC, as well as PPR of AMPAR-EPSC, were also unchanged in MSNs from Cul3$^{f/f}$ + Cre(STR) mice (Supplementary Fig. 4d and e). These data suggest that Cul3 deletion does not induce significant alterations of synaptic responses in striatal medium spiny neurons.

Forebrain Cul3 deficiency leads to increased RhoA expression and decreased spine density in PFC

Next, we examined the impact of forebrain Cul3 deficiency on protein expression and morphological features. One of the substrates of Cul3 is RhoA [33], a key regulator of actin cytoskeleton, dendrite development, spine formation, and axonal growth [33–37]. It has been speculated that Cul3/Kctd13-mediated RhoA ubiquitination underlies the ASD-associated developmental deficits associated with 16p11.2 deletion or duplication [38]. Our Western blotting analyses found that the level of RhoA was significantly increased in frontal cortex of Cul3$^{f/-}$ mice (Fig. 4a), while another member of the Rho family of GTPases, Rac1, was not
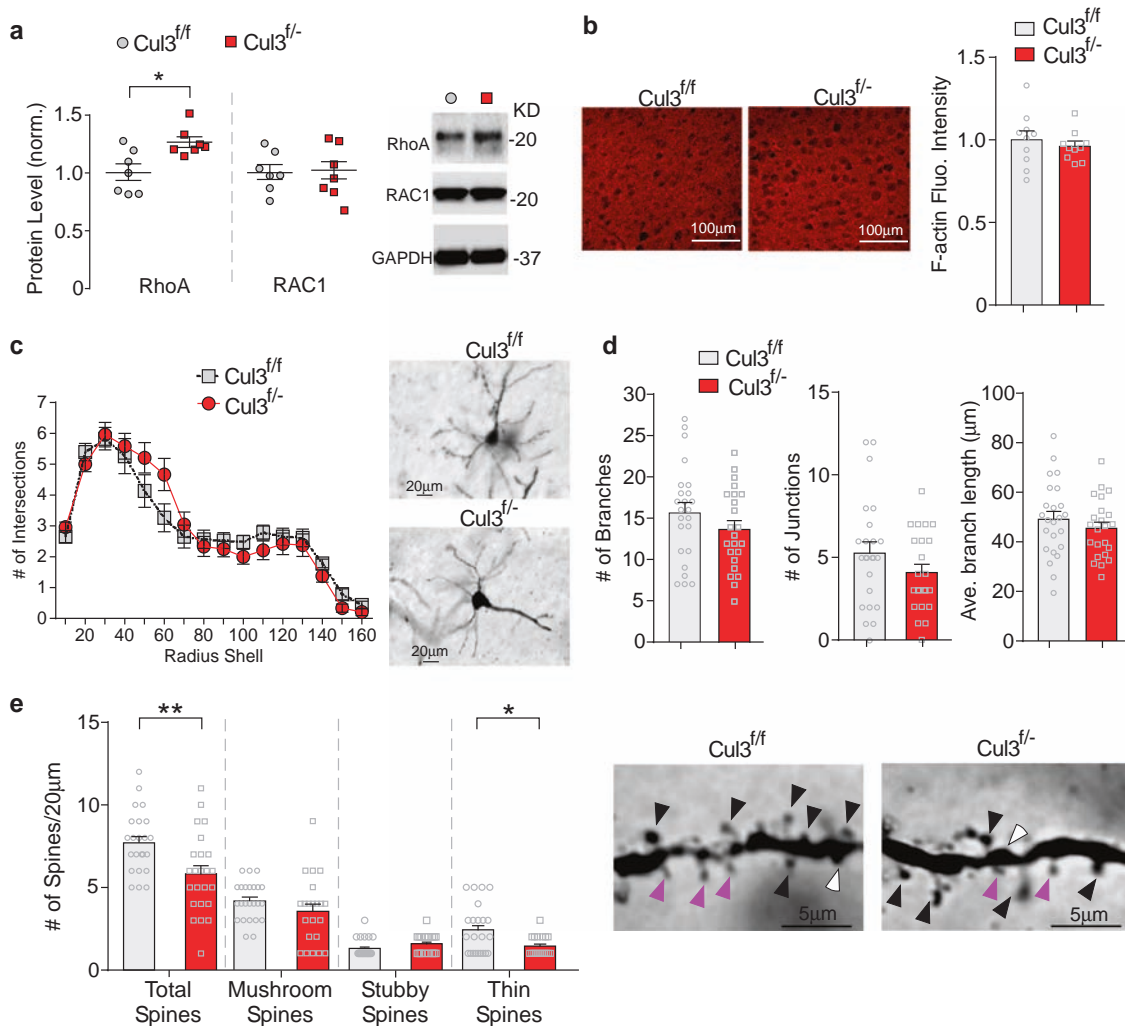
Fig. 4 Forebrain Cul3 deficiency leads to an increased level of RhoA and reduced density of dendritic spines in PFC pyramidal neurons. **a** Western blot quantifications of RhoA and Rac1 in PFC lysates from Cul3$^{f/f}$ ($n = 7$) and Cul3$^{f/-}$ ($n = 7$) mice. RhoA: $t(12) = 3.1$, $p = 0.01$, t test. **b** Image of F-actin (phalloidin) staining and quantification of fluorescent intensity in PFC slices from Cul3$^{f/f}$ ($n = 7$) and Cul3$^{f/-}$ ($n = 7$) mice. **c** Plot of dendritic branching as measured by Sholl analysis in PFC pyramidal neurons from Cul3$^{f/f}$ ($n = 24$ dendrites/5 mice) and Cul3$^{f/-}$ ($n = 24$ dendrites/5 mice). Representative Golgi-stained neurons are also shown. **d** Plot of branch numbers, junction numbers, and average branch length in Cul3$^{f/f}$ ($n = 24$ dendrites/5 mice) and Cul3$^{f/-}$ ($n = 24$ dendrites/5 mice). **e** Plot of densities of total, mushroom, stubby and thin spines in PFC pyramidal neurons from Cul3$^{f/f}$ ($n = 24$ dendrites/5 mice) and Cul3$^{f/-}$ ($n = 24$ dendrites/5 mice). Total spines: $U = 150.5$, $p = 0.004$; mushroom spines: $U = 198$, $p = 0.1$; thin spines: $U = 131.0$, $p = 0.04$, Mann–Whitney test. Representative images of dendritic spines are also shown. Black arrowheads: mushroom spines; fuchsia arrowheads: thin spines; white arrowheads: stubby spines. In all figures, *$p < 0.05$, **$p < 0.01$

significantly changed by Cul3 deficiency (Fig. 4a). However, immunostaining of F-actin with phalloidin did not find significant changes in Cul3$^{f/-}$ mice, compared to Cul3$^{f/f}$ mice (Fig. 4b).

To evaluate whether the RhoA increase in Cul3$^{f/-}$ mice might induce morphological changes in dendrites and spines, we performed Golgi staining. Layer 5 PFC pyramidal neurons, which show the clearest deficits in autistic children [16], were examined. Sholl analyses of these neurons from Cul3$^{f/-}$ mice did not find significant changes in dendritic arborization (Fig. 4c), or the number and length of dendritic branches (Fig. 4d). However, the density of total spines was significantly reduced in Cul3$^{f/-}$ mice (Fig. 4e). By classifying the spines into three subtypes: mushroom, thin and stubby, we found a trend of reduction in the density of mushroom spines and a significant reduction of the density of thin spines in Cul3$^{f/-}$ mice (Fig. 4e).

Brain region-specific Cul3 deficiency leads to large-scale alterations of protein expression

Since Cul3 is a core component of the E3 ubiquitin ligase complex, loss of Cul3 can result in the alteration of multiple
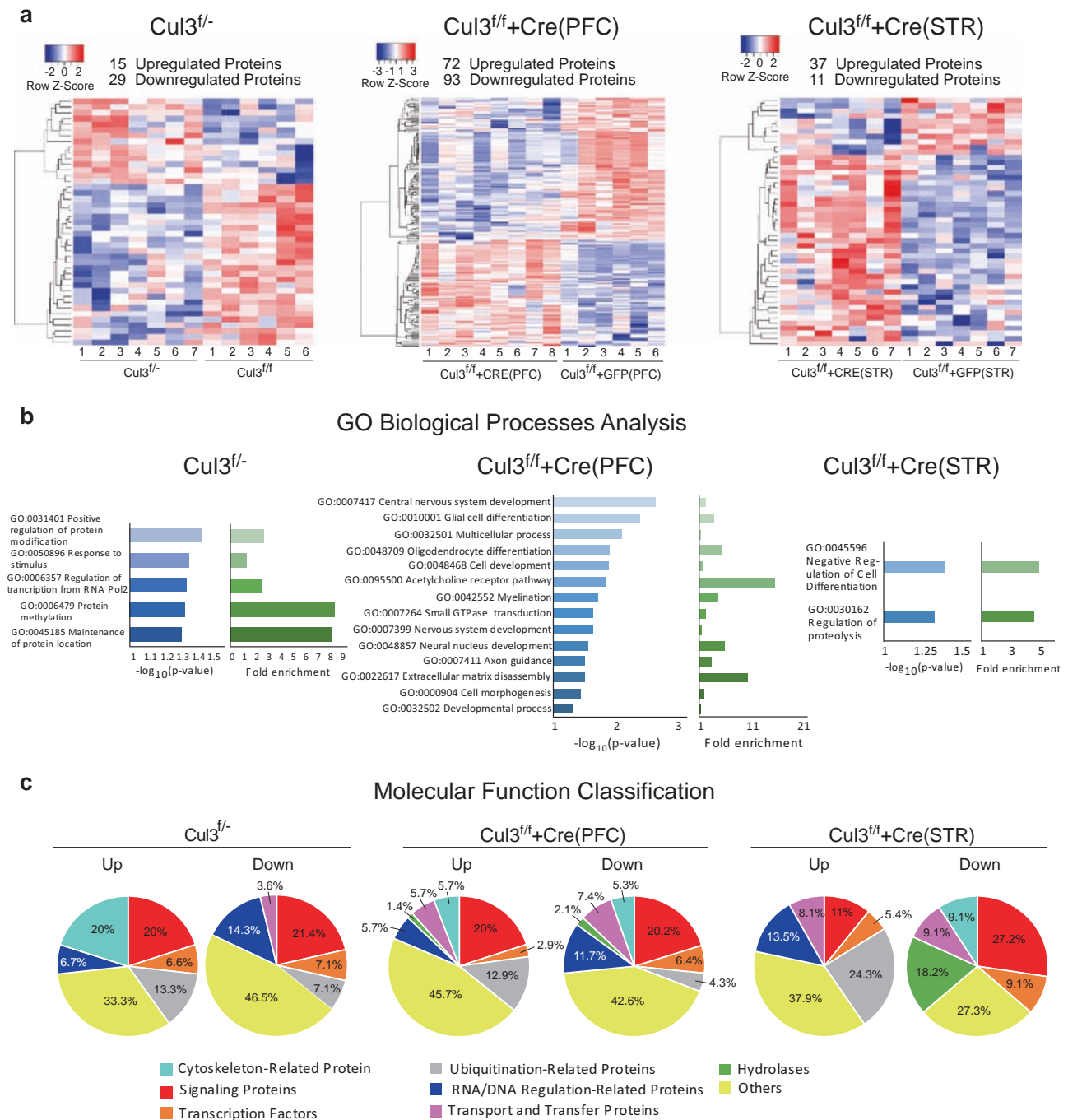
Fig. 5 Brain region-specific Cul3 deficiency induces large-scale changes of protein expression. **a** Heat maps of differentially expressed proteins identified by proteomic analyses in Cul3$^{f/-}$ ($n = 7$), Cul3$^{f/f}$ + Cre(PFC) ($n = 8$), and Cul3$^{f/f}$ + Cre(STR) ($n = 7$) mice, compared to respective controls (Cul3$^{f/f}$ ($n = 6$), Cul3$^{f/f}$ + GFP(PFC) ($n = 6$), and Cul3$^{f/f}$ + GFP(STR) ($n = 7$) mice. **b** Biological processes-based GO analysis of the misregulated proteins in Cul3$^{f/-}$, Cul3$^{f/f}$ + Cre(PFC), and Cul3$^{f/f}$ + Cre(STR) mice. **c** Molecular function classification of the upregulated (Up) and downregulated (Down) proteins in Cul3$^{f/-}$, Cul3$^{f/f}$ + Cre(PFC), and Cul3$^{f/f}$ + Cre(STR) mice

proteins, which may collectively contribute to the structural and functional changes and behavioral phenotypes associated with autism. To test this, we performed high-throughput proteomic analysis to identify differentially expressed proteins in mice with forebrain Cul3 deficiency, as well as in mice with PFC- or striatum-specific deletion of Cul3.

As shown in Fig. 5a, forebrain Cul3 deficiency led to 15 upregulated and 29 downregulated proteins in frontal cortex from Cul3$^{f/-}$ mice, compared to Cul3$^{f/f}$ mice (Supplementary Table 1); PFC-specific deletion of Cul3 generated 72 upregulated and 93 downregulated proteins in PFC from Cul3$^{f/f}$ + Cre(PFC) mice, compared to
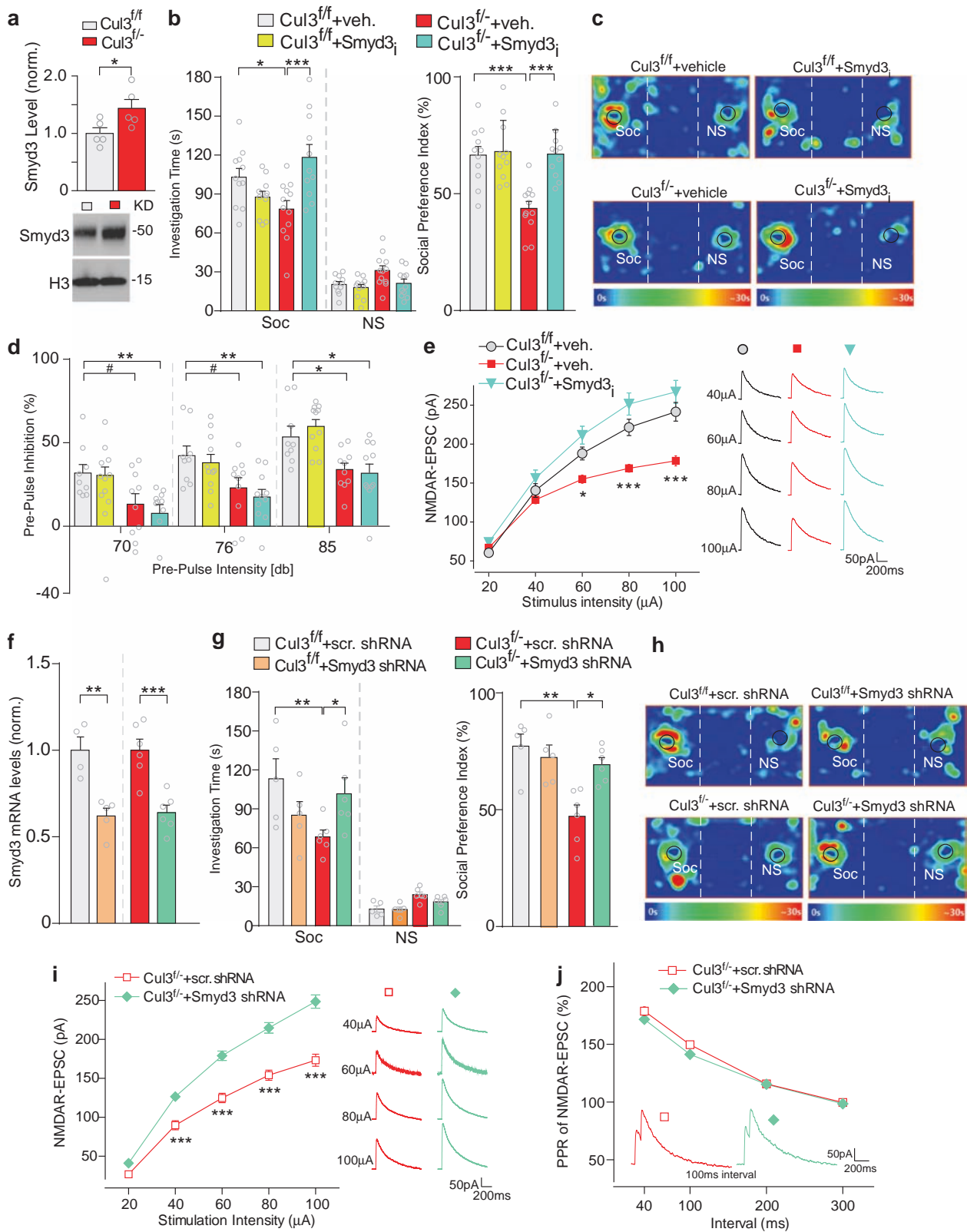
Cul3^{f/f} + GFP(PFC) mice (Supplementary Table 2); while striatum-specific deletion of Cul3 produced 37 upregulated and 11 downregulated proteins in striatum from Cul3^{f/f} + Cre(STR) mice, compared to Cul3^{f/f} + GFP (STR) mice (Supplementary Table 3). This proteomic analysis has revealed multiple new targets of Cul3,

including those linked to neurodevelopmental disorders, such as ASD, fragile X syndrome (FXS), and intellectual disability (ID).

Gene ontology analyses indicated that these misregulated proteins by region-specific Cul3 deficiency had different profiles of over-representation in biological processes (Fig. 5b). In forebrain Cul3-deficient mice (Cul3$^{f/-}$), the differentially expressed proteins were enriched in processes like protein methylation and maintenance of protein location. In mice with PFC deletion of Cul3, Cul3$^{f/f}$ + Cre (PFC), the differentially expressed proteins were highly involved in the acetylcholine receptor pathway, extracellular matrix disassembly, neural nucleus development, oligodendrocyte differentiation and myelination. In mice with striatal deletion of Cul3, Cul3$^{f/f}$ + Cre(STR), the differentially expressed proteins were enriched in processes like negative regulation of cell differentiation and regulation of proteolysis.

Molecular function (MF) classification of these misregulated proteins by region-specific Cul3 deficiency revealed distinct and convergent patterns (Fig. 5c). In forebrain Cul3-deficient mice (Cul3$^{f/-}$), cytoskeleton, signaling and ubiquitination-related proteins represented ~1/2 of the upregulated proteins, while signaling, RNA/DNA regulation, ubiquitination-related proteins and transcription factors represented ~1/2 of the downregulated proteins. In mice with PFC deletion of Cul3, Cul3$^{f/f}$ + Cre(PFC), differentially expressed proteins were scattered among multiple groups, with signaling and ubiquitination-related proteins making up ~1/3 of the upregulated proteins, and signaling and RNA/DNA regulation proteins making up ~1/3 of the downregulated proteins. In mice with striatal deletion of Cul3, Cul3$^{f/f}$ + Cre(STR), the upregulated proteins were mainly related to signaling, transport/transfer, ubiquitination and RNA/DNA regulation, while the downregulated proteins were mainly under the same categories in addition to hydrolases and cytoskeleton-related proteins.

To further understand the impact of Cul3 deficiency on cell physiology, we performed an interactome network analysis, based on identified and predicted interactions between the misregulated proteins and key intermediaries. The interactome networks were built using differentially expressed proteins in region-specific Cul3-deficient mice as main nodes (clustered based on MF classification).

In Cul3$^{f/-}$ mice, the upregulated proteins had a lower connectivity than downregulated proteins (Supplementary Fig. 5a and b). A high degree of connectivity was found in upregulated proteins like Ncor2, Syap1, Sun1, and Lgals1, and in downregulated proteins like ERCC2, Nrp1, and UNC119. In Cul3$^{f/f}$ + Cre(PFC) mice, the degree of connectivity was higher in upregulated proteins, despite the bigger number of downregulated proteins (Supplementary Fig. 5c and d). High connectivity was found in upregulated proteins like Grb10, Lamc1, Lama1, and Bad, and in downregulated proteins as Hspg2, Ercc2, Bcl11b, Lyst, Prom1, Mbp, Vldlr, Efnb2, and Plp1. In Cul3$^{f/f}$ + Cre(STR) mice, the connectivity was substantially higher in the upregulated proteins, compared to the downregulated proteins (Supplementary Fig. 5e and f). High connectivity was found in upregulated proteins like Stat1, Grb10, Psme1, Btbd10, and Lamb1. These analyses give us a more comprehensive view of how Cul3 deletions could influence protein interactions, which may underlie the behavioral abnormalities associated with ASD.

Inhibition of the upregulated Smyd3 in forebrain *Cul3*-deficient mice rescues social deficits and NMDAR hypofunction in PFC

Large-scale proteomic studies have provided non-biased analysis of protein changes, which correlates with behavioral and electrophysiological alterations. Next, we sought to find out the causal role of identified top candidates in autism pathophysiology. From the proteomic data, one of the upregulated proteins by forebrain Cul3 deficiency is Smyd3, a

histone methyltransferase catalyzing H3K4me3, which is linked to gene activation. The upregulation of Smyd3 protein level in Cul3$^{f/-}$ mice was confirmed by Western blot analyses of frontal cortical tissue (Fig. 6a). It is of particular interest, because postmortem frontal cortex from autism patients exhibits altered trimethylated H3K4 landscapes [39]. Histone-modifying enzymes that mediate post-translational lysine methylation/demethylation modifications of histones have been identified as the most prominent autism risk factors [2]. The upregulated Smyd3 could contribute to the dysregulation of gene expression, leading to molecular alterations and behavioral deficits in Cul3-deficient mice.

To test this, we examined the impact of Smyd3 inhibition on behavioral phenotypes in Cul3$^{f/-}$ mice. One specific Smyd3 inhibitor is the small molecule compound BCI-121, which competes against histones for Smyd3 binding, reduces H3K4 di- and tri-methylation and downregulates Smyd3 target genes transcription [40]. The systemic administration of BCI-121 (1 mg/kg, i.p., once daily for 3 days) significantly reduced the level of H3K4me3 in PFC (Supplementary Fig. 6), suggesting the effectiveness of this compound in regulating histone methylation in the brain. Cul3$^{f/-}$ mice treated with the Smyd3 inhibitor BCI-121 (Smyd3$_i$, 1 mg/kg, i.p., 3×) exhibited significantly improved social behaviors, as indicated by the increased time interacting with the social stimulus and the higher social preference index in three-chamber sociability tests, compared to vehicle-treated Cul3$^{f/-}$ mice (Fig. 6b, c). However, the Smyd3 inhibitor failed to rescue PPI deficits in Cul3$^{f/-}$ mice (Fig. 6d). Moreover, electrophysiological studies found that PFC pyramidal neurons from Smyd3$_i$-treated Cul3$^{f/-}$ mice had significantly elevated NMDAR-mediated synaptic currents (Fig. 6e), indicating the rescue of PFC NMDAR hypofunction, which is probably linked to the amelioration of social impairment.

To confirm that these rescue effects were unequivocally related to Smyd3 inhibition and not an off-target effect of BCI-121, we knocked down Smyd3 expression in PFC of Cul3$^{f/-}$ mice by injecting lentiviral particles containing a shRNA sequence against Smyd3, and examined social behavior and NMDAR function. Compared to a scrambled control shRNA, the Smyd3 shRNA caused a significant in vivo reduction of Smyd3 expression in PFC (Fig. 6f). In Cul3$^{f/-}$ mice with PFC injection of Smyd3 shRNA, significant improvements were observed in the social interaction time and social preference index (Fig. 6g, h), as well as NMDAR-EPSC amplitudes recorded in PFC pyramidal neurons (Fig. 6i). The PPR of NMDAR-EPSC was unchanged by Smyd3 knockdown (Fig. 6j). Taken together, it suggests that Smyd3 could be one of the major downstream targets of Cul3 that controls the manifestation of some autistic phenotypes by Cul3 deficiency.

Discussion

In this study, we have provided the first pre-clinical evidence that Cul3 deficiency can produce two main behavioral abnormalities observed in ASD: impaired social interaction and repetitive behaviors, supporting the identification of Cul3 as one of the high-confidence risk genes for autism [2, 38]. Interestingly, different behavioral deficits are manifested in mice with brain region-specific deletions of Cul3. The ASD-like social deficits are mainly linked to Cul3 deficiency in the forebrain or PFC, a brain region critical for social cognition and social preference [24, 41, 42]. On the other hand, the elevated repetitive grooming behavior is primarily associated with Cul3 deficiency in the striatum, a brain region important for habit formation and stereotypic behaviors [28–30, 43]. These results have identified Cul3 as a key molecule that may be responsible for the involvement of these brain regions in distinct behavioral phenotypes.

Electrophysiological changes in synaptic function and neuronal excitability induced by region-specific Cul3 deletion correlate well with the behavioral phenotypes. Cul3 deficiency in the forebrain or PFC has led to NMDAR hypofunction, a synaptic change often found in other genetic models of autism, such as those with Shank3 or Shank2 deficiency [24, 42, 44] and 16p11.2 deletion mice [45]. Cul3 deficiency in the striatum has led to the reduced AP firing frequency of MSNs, most prominently the putative D1-positive striatonigral MSNs. Other than these functional alterations, forebrain Cul3-deficient mice exhibit decreased spine density, which could be due to the elevated RhoA expression, since RhoA activity negatively regulates spine formation [36]. Mice with the deletion of Kctd13, one of the Cul3 adapters, also have increased RhoA [46]. However, Kctd13 knockout mice do not exhibit ASD-like core behavioral symptoms [46], suggesting that RhoA aberration alone is not sufficient to generate ASD phenotypes.

As a core component of the E3 ubiquitin ligase complex, Cul3 can be involved in the degradation of many proteins by pairing with ~90 distinct substrate adapters [6, 47]. Although Cul3 is ubiquitously expressed, our proteomic analyses have revealed different sets of proteins misregulated by Cul3 deficiency in different brain regions at different time points. Forebrain deletion of Cul3 during embryonic stages led to the upregulation of proteins like histone methyltransferase Smyd3 and transcription factor Ncor2, both of which can generate broad changes in gene expression. It also produced the downregulation of proteins linked to ID, autism, and neuronal development like Ercc2, Stard9, Tbc1d23, Lrba, Paf1, MSK1, and Dusp15.

PFC-specific deletion of Cul3 at postnatal stages led to the upregulation of proteins related to cholinergic signaling (Chrm1 and Agrn), cortical development (Pls1, Lamb2, and

Lamc1) and DNA modulators (Polr2a and Glyr1), as well as the downregulation of proteins related to autism, FXS and ID, such as Ercc2, Dock1, Ermn, Kcnt1, Pcdh19, and Trim33. Striatum-specific deletion of Cul3 produced the upregulation of transcriptional regulators like Stat1 and Ubtf, as well as RNA processing and transport proteins like Prpf3 and Stau2.

Given the substantial differences in neuronal composition and connectivity between PFC and STR, the different profiles of misregulated proteins by Cul3 deficiency are within expectation. However, many of these differentially expressed proteins also have common molecular functions, such as cell signaling, protein ubiquitination, and gene transcription. These proteomic data suggest that Cul3 deficiency could have a broad impact in brain physiology by affecting multiple proteins, and manipulation of an individual or a few misregulated proteins is unlikely to completely ameliorate the behavioral and physiological effects of Cul3 deletion. However, some key molecules that are multifunctional or have broad interactions with other differentially expressed proteins may play more prominent roles in controlling different symptoms. Our data with Smyd3 inhibition is promising. More studies will be carried out to examine the impact of region-specific normalization of key proteins in Cul3 networks.

Overall, this study has provided the first evidence regarding the involvement of Cul3 in core behaviors of ASD. We have also revealed the Cul3 deficiency-induced changes in cortico-striatal neuronal functioning that correlate with the behavioral outputs. Proteomic analysis has identified the network of proteins altered by Cul3 deletion, which offers both mechanistic insights into the role of Cul3 in autism and potential molecular targets of Cul3 for therapeutic interventions.

Data availability

Proteomic data will be deposited in a public repository. The access number and the dataset will be available for access.

Compliance with ethical standards

References

1. de la Torre-Ubieta L, Won H, Stein JL, Geschwind DH. Advancing the understanding of autism disease mechanisms through genetics. Nat Med. 2016;22:345–61.
2. De Rubeis S, He X, Goldberg AP, Poultney CS, Samocha K, Cicek AE, et al. Synaptic, transcriptional and chromatin genes disrupted in autism. Nature. 2014;515:209–15.
3. O'Roak BJ, Vives L, Girirajan S, Karakoc E, Krumm N, Coe BP, et al. Sporadic autism exomes reveal a highly interconnected protein network of de novo mutations. Nature. 2012;485:246–50.
4. Kong A, Frigge ML, Masson G, Besenbacher S, Sulem P, Magnusson G, et al. Rate of de novo mutations and the importance of father's age to disease risk. Nature. 2012;488:471–5.
5. Stessman HA, Xiong B, Coe BP, Wang T, Hoekzema K, Fenckova M, et al. Targeted sequencing identifies 91 neurodevelopmental-disorder risk genes with autism and developmental-disability biases. Nat Genet. 2017;49:515–26.
6. Genschik P, Sumara I, Lechner E. The emerging family of CULLIN3-RING ubiquitin ligases (CRL3s): cellular functions and disease implications. EMBO J. 2013;32:2307–20.
7. Pinkas DM, Sanvitale CE, Bufton JC, Sorrell FJ, Solcan N, Chalk R, et al. Structural complexity in the KCTD family of Cullin3-dependent E3 ubiquitin ligases. Biochem J. 2017;474:3747–61.
8. Dubiel W, Dubiel D, Wolf DA, Naumann M. Cullin 3-based ubiquitin ligases as master regulators of mammalian cell differentiation. Trends Biochem Sci. 2018;43:95–107.
9. Chen HY, Liu CC, Chen RH. Cul3-KLHL20 ubiquitin ligase: physiological functions, stress responses, and disease implications. Cell Div. 2016;11:5.
10. Weiss LA, Shen Y, Korn JM, Arking DE, Miller DT, Fossdal R, et al. Association between microdeletion and microduplication at 16p11.2 and autism. N Engl J Med. 2008;358:667–75.
11. Kumar RA, KaraMohamed S, Sudi J, Conrad DF, Brune C, Badner JA, et al. Recurrent 16p11.2 microdeletions in autism. Hum Mol Genet. 2008;17:628–38.
12. McCarthy SE, Makarov V, Kirov G, Addington AM, McClellan J, Yoon S, et al. Microduplications of 16p11.2 are associated with schizophrenia. Nat Genet. 2009;41:1223–U1285.
13. Singer JD, Gurian-West M, Clurman B, Roberts JM. Cullin-3 targets cyclin E for ubiquitination and controls S phase in mammalian cells. Genes Dev. 1999;13:2375–87.
14. Ha S, Sohn IJ, Kim N, Sim HJ, Cheon KA. Characteristics of brains in autism spectrum disorder: structure, function and connectivity across the lifespan. Exp Neurobiol. 2015;24:273–84.
15. Hernandez LM, Rudie JD, Green SA, Bookheimer S, Dapretto M. Neural signatures of autism spectrum disorders: insights into brain network dynamics. Neuropsychopharmacology. 2015;40:171–89.
16. Stoner R, Chow ML, Boyle MP, Sunkin SM, Mouton PR, Roy S, et al. Patches of disorganization in the neocortex of children with autism. N Engl J Med. 2014;370:1209–19.
17. Schubert D, Martens GJ, Kolk SM. Molecular underpinnings of prefrontal cortex development in rodents provide insights into the etiology of neurodevelopmental disorders. Mol Psychiatry. 2015;20:795–809.

18. Shepherd GM. Corticostriatal connectivity and its role in disease. Nat Rev Neurosci. 2013;14:278–91.

19. McEvoy JD, Kossatz U, Malek N, Singer JD. Constitutive turnover of cyclin E by Cul3 maintains quiescence. Mol Cell Biol. 2007;27:3651–66.

20. Gulisano M, Broccoli V, Pardini C, Boncinelli E. Emx1 and Emx2 show different patterns of expression during proliferation and differentiation of the developing cerebral cortex in the mouse. Eur J Neurosci. 1996;8:1037–50.

21. Gorski JA, Talley T, Qiu M, Puelles L, Rubenstein JL, Jones KR, et al. Cortical excitatory neurons and glia, but not GABAergic neurons, are produced in the Emx1-expressing lineage. J Neurosci. 2002;22:6309–14.

22. Perry W, Minassian A, Lopez B, Maron L, Lincoln A. Sensorimotor gating deficits in adults with autism. Biol Psychiatry. 2007;61:482–6.

23. Brumback AC, Ellwood IT, Kjaerby C, Iafrati J, Robinson S, Lee AT, et al. Identifying specific prefrontal neurons that contribute to autism-associated abnormalities in physiology and social behavior. Mol Psychiatry. 2017;23:2078–89.

24. Duffney LJ, Zhong P, Wei J, Matas E, Cheng J, Qin L, et al. Autism-like deficits in Shank3-deficient mice are rescued by targeting actin regulators. Cell Rep. 2015;11:1400–13.

25. Tebartz van Elst L, Maier S, Fangmeier T, Endres D, Mueller GT, Nickel K, et al. Disturbed cingulate glutamate metabolism in adults with high-functioning autism spectrum disorder: evidence in support of the excitatory/inhibitory imbalance hypothesis. Mol Psychiatry. 2014;19:1314–25.

26. Willsey AJ, Sanders SJ, Li M, Dong S, Tebbenkamp AT, Muhle RA, et al. Coexpression networks implicate human midfetal deep cortical projection neurons in the pathogenesis of autism. Cell. 2013;155:997–1007.

27. Ajram LA, Horder J, Mendez MA, Galanopoulos A, Brennan LP, Wichers RH, et al. Shifting brain inhibitory balance and connectivity of the prefrontal cortex of adults with autism spectrum disorder. Transl Psychiatry. 2017;7:e1137.

28. Fuccillo MV. Striatal circuits as a common node for autism pathophysiology. Front Neurosci. 2016;10:27.

29. Burguiere E, Monteiro P, Mallet L, Feng G, Graybiel AM. Striatal circuits, habits, and implications for obsessive-compulsive disorder. Curr Opin Neurobiol. 2015;30:59–65.

30. Langen M, Bos D, Noordermeer SD, Nederveen H, van Engeland H, Durston S. Changes in the development of striatum are involved in repetitive behavior in autism. Biol Psychiatry. 2014;76:405–11.

31. Kreitzer AC, Malenka RC. Endocannabinoid-mediated rescue of striatal LTD and motor deficits in Parkinson's disease models. Nature. 2007;445:643–7.

32. Cepeda C, Andre VM, Yamazaki I, Wu N, Kleiman-Weiner M, Levine MS. Differential electrophysiological properties of dopamine D1 and D2 receptor-containing striatal medium-sized spiny neurons. Eur J Neurosci. 2008;27:671–82.

33. Chen Y, Yang Z, Meng M, Zhao Y, Dong N, Yan H, et al. Cullin mediates degradation of RhoA through evolutionarily conserved BTB adaptors to control actin cytoskeleton structure and cell movement. Mol Cell. 2009;35:841–55.

34. Zhang H, Macara IG. The PAR-6 polarity protein regulates dendritic spine morphogenesis through p190 RhoGAP and the Rho GTPase. Dev Cell. 2008;14:216–26.

35. Yan Z, Kim E, Datta D, Lewis DA, Soderling SH. Synaptic actin dysregulation, a convergent mechanism of mental disorders? J Neurosci. 2016;36:11411–7.

36. Tashiro A, Minden A, Yuste R. Regulation of dendritic spine morphology by the rho family of small GTPases: antagonistic roles of Rac and Rho. Cereb Cortex. 2000;10:927–38.

37. Quassollo G, Wojnacki J, Salas DA, Gastaldi L, Marzolo MP, Conde C, et al. A RhoA signaling pathway regulates dendritic golgi outpost formation. Curr Biol. 2015;25:971–82.

38. Lin GN, Corominas R, Lemmens I, Yang X, Tavernier J, Hill DE, et al. Spatiotemporal 16p11.2 protein network implicates cortical late mid-fetal brain development and KCTD13-Cul3-RhoA pathway in psychiatric diseases. Neuron. 2015;85:742–54.

39. Shulha HP, Cheung I, Whittle C, Wang J, Virgil D, Lin CL, et al. Epigenetic signatures of autism: trimethylated H3K4 landscapes in prefrontal neurons. Arch Gen Psychiatry. 2012;69:314–24.

40. Peserico A, Germani A, Sanese P, Barbosa AJ, Di Virgilio V, Fittipaldi R, et al. A SMYD3 small-molecule inhibitor impairing cancer cell growth. J Cell Physiol. 2015;230:2447–60.

41. Amodio DM, Frith CD. Meeting of minds: the medial frontal cortex and social cognition. Nat Rev Neurosci. 2006;7:268–77.

42. Qin L, Ma K, Wang ZJ, Hu Z, Matas E, Wei J, et al. Social deficits in Shank3-deficient mouse models of autism are rescued by histone deacetylase (HDAC) inhibition. Nat Neurosci. 2018;21:564–75.

43. Peca J, Feliciano C, Ting JT, Wang W, Wells MF, Venkatraman TN, et al. Shank3 mutant mice display autistic-like behaviours and striatal dysfunction. Nature. 2011;472:437–42.

44. Won H, Lee HR, Gee HY, Mah W, Kim JI, Lee J, et al. Autistic-like social behaviour in Shank2-mutant mice improved by restoring NMDA receptor function. Nature. 2012;486:261–5.

45. Wang W, Rein B, Zhang F, Tan T, Zhong P, Qin LY, et al. Chemogenetic activation of prefrontal cortex rescues synaptic and behavioral deficits in a mouse model of 16p11.2 deletion syndrome. J Neurosci. 2018;38:5939–48.

46. Escamilla CO, Filonova I, Walker AK, Xuan ZX, Holehonnur R, Espinosa F, et al. Kctd13 deletion reduces synaptic transmission via increased RhoA. Nature. 2017;551:227–31.

47. McGourty CA, Akopian D, Walsh C, Gorur A, Werner A, Schekman R, et al. Regulation of the CUL3 ubiquitin ligase by a calcium-dependent co-adaptor. Cell. 2016;167:525–38 e514.